**Research Article**

# Improved conductivity and capacitance of interdigital carbon microelectrodes through integration with carbon nanotubes for micro-supercapacitors

Yanjuan Yang[1], Liang He[1] (✉), Chunjuan Tang[1,2], Ping Hu[1], Xufeng Hong[1], Mengyu Yan[1], Yixiao Dong[1], Xiaocong Tian[1], Qiulong Wei[1], and Liqiang Mai[1] (✉)

[1] *State Key Laboratory of Advanced Technology for Materials Synthesis and Processing, Wuhan University of Technology, Wuhan 430070, China*

[2] *Department of Mathematics and Physics, Luoyang Institute of Science and Technology, Luoyang 471023, China*

## ABSTRACT

In the last decade, pyrolyzed-carbon-based composites have attracted much attention for their applications in micro-supercapacitors. Although various methods have been investigated to improve the performance of pyrolyzed carbons, such as conductivity, energy storage density and cycling performance, effective methods for the integration and mass-production of pyrolyzed-carbon-based composites on a large scale are lacking. Here, we report the development of an optimized photolithographic technique for the fine micropatterning of photoresist/chitosan-coated carbon nanotube (CHIT-CNT) composite. After subsequent pyrolysis, the fabricated carbon/CHIT-CNT microelectrode-based micro-supercapacitor has a high capacitance (6.09 mF·cm$^{-2}$) and energy density (4.5 mWh·cm$^{-3}$) at a scan rate of 10 mV·s$^{-1}$. Additionally, the micro-supercapacitor has a remarkable long-term cyclability, with 99.9% capacitance retention after 10,000 cyclic voltammetry cycles. This design and microfabrication process allow the application of carbon microelectromechanical system (C-MEMS)-based micro-supercapacitors due to their high potential for enhancing the mechanical and electrochemical performance of micro-supercapacitors.

## 1   Introduction

Supercapacitors (also called electrochemical capacitors) have many applications in electrical energy storage and power harvesting because of their high power densities, fast charge/discharge capabilities, and long cycle lifetimes [1, 2]. Based on the mechanism of energy storage, supercapacitors can be divided into two types: electric double layer capacitors (EDLCs) and pseudocapacitors. The former store energy by ion adsorption on the interface of high-surface-area electrodes and the ion-containing electrolyte [3],

whereas the latter store energy through fast surface redox reactions in the active material [3–6]. Recent demand of thin and light micro-supercapacitors for portable electronic devices has made supercapacitors a popular type of power source and energy storage unit [7–14]. Carbonaceous materials, such as activated carbon, carbon nanotubes (CNTs) and graphene, are important and essential electrode materials for use in micro-supercapacitors [2]. In particular, porous carbon is often considered the most important EDLC electrode material because of its abundance, high surface area, well-developed manufacturing process, and excellent cycling stability, however, its conductivity is relatively poor [2, 5]. For carbon-based materials, CNTs are popular choices, often used to enhance the performance of electrode materials; this performance enhancement is due to the hollow structure of CNTs, which results in a highly accessible surface area, excellent conductivity, and structural stability; enabling fast ion and electron transport [15–17]. Various methods to modify CNTs have been developed to increase the performance of CNT-based electrochemical energy storage devices [4, 18, 19]. Of these effective modification methods, coating CNTs with chitosan is popular and has two main advantages. (1) To maintain the good conductivity of CNT materials, the CNTs must be well dispersed. One method of improving dispersibility is hydrophilization of the CNTs by introducing of hydrophilic functional groups to the surface; however, there are no direct chemical processes to achieve this [20]. Instead, chitosan can be used like a surfactant, covering the CNTs and improving their dispersibility. (2) In addition, chitosan contains nitrogen, allowing doping of carbon-based supercapacitor during the pyrolysis process. Furthermore, nitrogen doping can enhance the capacitance of carbon-based super-capacitors, which is an effect that results from robust redox reactions at nitrogen-associated defects [3].

In the past decades, many efforts have been made to fabricate high-performance carbon-microstructure-based micro-supercapacitors. Kaempgen et al. fabricated thin-film supercapacitors by spraying a stable suspension of single-walled CNT (SWCNT) onto a polyethylene-terphthalate (PET) substrate substrate, resulting in an electrode with high energy (6 Wh·kg⁻¹) and power densities (23 kW·kg⁻¹) when using a

hydrogel electrolyte [15]. Shen et al. fabricated an on-chip device based on microfabrication technologies [16]. In their work, electrode materials containing composites ($MnO_2$ as the positive electrode and activated carbon as the negative electrode) were injected into interdigitating channels etched on the silicon substrate. The asymmetric supercapacitor had a large voltage range of 1.5 V and a high capacitance (30 mF·cm⁻²).

Microfabrication technologies used to prepare micro-supercapacitors include photolithography, electrodeposition, as well as dip and dry [7, 10, 12]. As an example of an effective microfabrication process, carbon-based microelectromechanical system (C-MEMS) technology is a unique platform combining different polymer fabrication techniques with pyrolysis or thermal degradation [21–27]. C-MEMS is a powerful approach to the large-scale microfabrication of carbon-based current collectors and electrodes for micro-supercapacitors [12, 13, 28–32]. However, for the microfabrication process, which is highly integrative and compatible with micromachining technologies, some substances and technologies should be avoided; for example, the deep etching of silicon using strong acids or alkalis and some binder materials that may affect the electrochemical performance of the device. Therefore, the development of a microfabrication process that facilitates the preparation of high-performance carbon microstructures with high compatibility, high repeatability, and at a large scale is necessary to allow the development of micro-supercapacitors.

Herein, we report the fabrication of photoresist/chitosan-coated CNT (CHIT-CNT) micropatterns by one-time optimized photolithography, as shown in Fig. 1. Our work is the first time that this type of microfabrication has been used with this kind of composite for micro-supercapacitor applications. The CHIT-CNT micropatterns are converted to a carbon (C)/CHIT-CNT microelectrode array and a current collector by pyrolysis, and the resulting micro-supercapacitor shows enhanced mechanical properties and electrical conductivity. Moreover, the micro-supercapacitor shows excellent electrochemical performance, with ultrahigh specific capacitance (6.09 mF·cm⁻² at a scan rate of 10 mV·S⁻¹) and cyclability (99.9% capacitance retention after 10,000 CV cycles at a scan rate of 1 V·s⁻¹).

**(a) Wafer cleaning**   **(b) Spin coating**   **(c) Photolithography**   **(d) Pyrolysis**
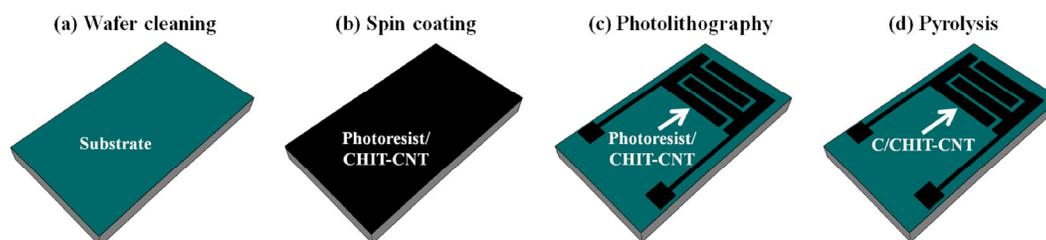
**Figure 1**   Microfabrication process of the C/CHIT-CNT micro-supercapacitor. (a) RCA cleaning of the Si/SiO₂ substrate. (b) Spin coating of photoresist/CHIT-CNT composite on the substrate. (c) Photolithography, development, and rinse. (d) Pyrolysis.

## 2   Experimental

### 2.1   Preparation of CHIT-CNT

CHIT-CNT was prepared by a controlled surface deposition process, as shown in Fig. S1 (in the Electronic Supplementary Material (ESM)). A typical preparation procedure is as follows [20]: Multi-walled CNTs (100 mg, MWCNT, purchased from XF NANO) were dispersed in a 100-mL chitosan solution (chitosan (0.1 g) dissolved in a 1% acetic acid solution (100 mL)) via ultrasonic agitation for 10 min followed by stirring for 1 h. Then, diluted ammonia was added into the CHIT-CNT solution, followed by formalin (40 mL). The solution was then heated at 60 °C for 20 min. Then, the CHIT-CNTs were washed with diluted acetic acid (1 vol.%), separated by centrifugation, and finally dried at 70 °C in an electric drying oven for 12 h. This controlled deposition process is used to improve the dispersion of CNTs in the photoresist [33–35]. In addition, unlike acid-treatment, the pristine structures of the CNTs are well preserved in the process of decoration with chitosan because no defects are introduced [36].

### 2.2   Fabrication process of the micro-supercapacitor

Interdigital microelectrodes (each having seven fingers with a size of 0.28 cm × 0.018 cm) were designed for their high area and volumetric utilization of the active materials [5, 7, 8]. The typical microfabrication process of patterned microelectrodes by the C-MEMS technique is shown in Fig. 1. This process consists of four steps. First, preparation of photoresist/CHIT-CNT composite and RCA cleaning of the Si/SiO₂ substrate (the thickness of oxide layer was 500 nm). Secondly, spin-coating of composite on the substrate. Thirdly, micropatterning of the interdigital microelectrodes.

Fourthly, pyrolysis, during which the photoresist/CHIT-CNT is converted to C/CHIT-CNT. The prepared CHIT-CNT was mixed in PR1-9000A photoresist (Futurrex) at 0.5 wt.% by continuous and simultaneous stirring and ultrasonic agitation for 10 h, yielding a uniform photoresist/CHIT-CNT composite. After standing for 2 h to allow air bubbles trapped in the composite to be lost, the composite was spin coated on a cleaned Si/SiO₂ wafer at 1,000 revolutions per minute (rpm) for 10 s and 6,000 rpm for 40 s, followed by 15 min soft-baking at 100 °C. The micropatterns were fabricated using optimized photolithography, development (conducted with RD6), and a longer rinse than the standard treatment used for PR1-9000A photoresist. After hard-baking at 115 °C for 10 min, the sample was placed in a hot-wall furnace for pyrolysis under N₂ atmosphere. The sample was heated at a rate of 2 °C·min⁻¹ from room temperature to 400 °C and held at this temperature for 30 min. Then, the sample was heated at the same rate to either 800, 900, or 1,000 °C and kept at this temperature for 1 h. After cooling to room temperature naturally, the preparation of the pyrolyzed-composite microelectrode micro-supercapacitor was complete. After pyrolysis at 900 °C, the thickness of C/CHIT-CNT microelectrode was ~1.2 μm, as determined by a surface profiler. Due to the excellent mechanical properties and electrical conductivity of C/CHIT-CNT, it can act not only as the electrode active material but also as the current collector. Microelectrodes with different materials (pure pyrolyzed carbon and C/pristine CNT) were also fabricated by a similar process.

### 2.3   Characterization

Scanning electron microscopy (SEM) images were collected with a JEOL JSM-7100F SEM at an acceleration

voltage of 15 kV. X-ray photoelectron spectroscopy (XPS) measurements were performed using a VG MultiLab 2000 instrument. Raman spectra were acquired using a Renishaw RM-1000 laser Raman microscope. Thermogravimetric (TG) measurements were performed using a Netzsch STA 449C simultaneous thermal analyzer at a heating rate of $10\ ^{\circ}C\cdot min^{-1}$ under $N_2$ atmosphere. The electrochemical performances were evaluated using an Autolab 302N combined with a probe station (Lake Shore, TTPX).

## 3    Results and discussion

### 3.1    Structural characterization

Figures 2(a) and 2(b) show SEM images of the pristine MWCNTs and CHIT-CNTs, respectively, showing their surface morphologies. The irregular surface of the CHIT-CNTs indicates that chitosan is uniformly coated on the CNTs. As shown in Fig. 2(c), the prepared CHIT-CNT is dispersed uniformly throughout the carbon after pyrolysis. The carbonization of the PR1-9000A photoresist was confirmed by high-resolution XPS in the C 1s region (Fig. 2(d)) and an XPS survey of the surface of the fabricated

microelectrode after pyrolysis at 900 °C (Fig. S2 in the ESM). Thermogravimetric analysis (TGA) of the PR1-9000A photoresist was carried out under $N_2$ atmosphere (Fig. 2(e)), and the weight retention at 800 °C was found to be ~16%; furthermore, there was no obvious weight loss at temperatures higher than 800 °C. In this work, temperatures of 800, 900, and 1,000 °C were selected to explore the optimal pyrolysis temperature.

Raman spectra of the C/CHIT-CNT microelectrodes formed by pyrolysis at 900 and 1,000 °C were measured to confirm the carbonaceous nature of the pyrolyzed samples, and these are shown in Fig. 2(f). Two broad peaks centered at ~1,320 (disorder-induced band, D-band) and ~1,600 $cm^{-1}$ (graphitic band, G-band) are clear in the two samples. The smaller intensity ratio of D/G band ($I_D/I_G$ = 1.06) after pyrolysis at 900 °C is indicative of the higher degree of graphitization and larger graphite crystallites of that composite compared to that pyrolyzed at 1,000 °C ($I_D/I_G$ = 1.13) [18].

### 3.2    Electrochemical characterization

Symmetric micro-supercapacitors formed of C/CHIT-CNT, pure pyrolyzed carbon, and C/pristine CNT
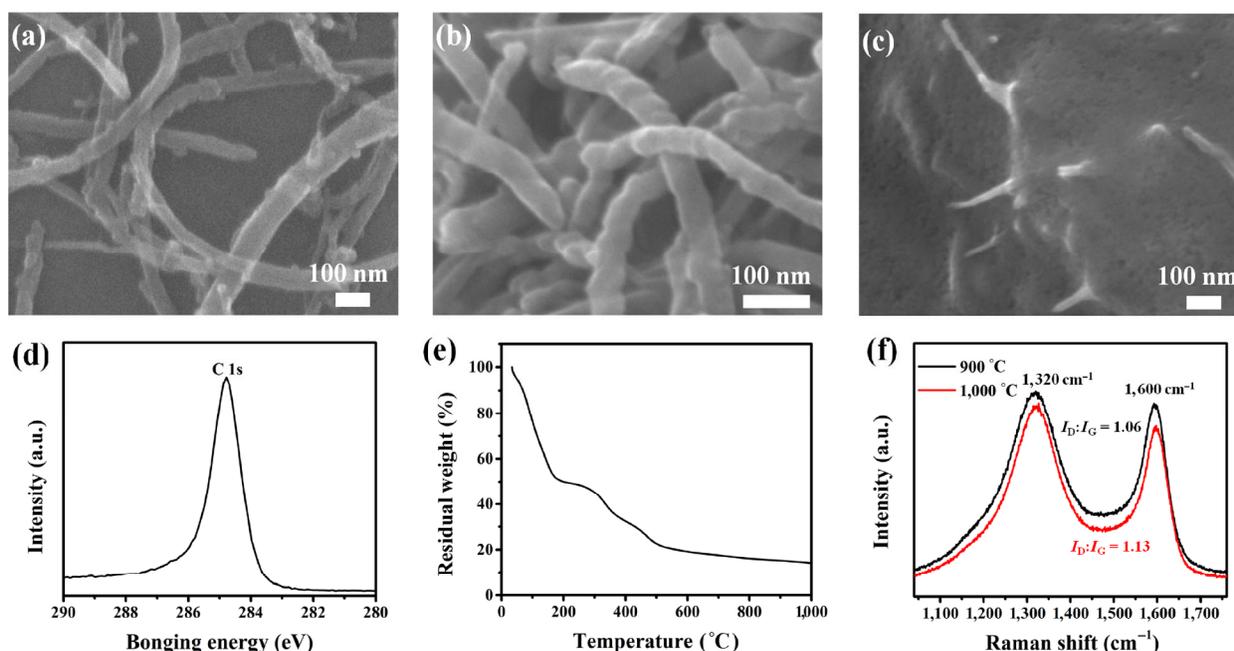


**Figure 2**    SEM images of (a) pristine CNTs, (b) CHIT-CNTs, and (c) C/CHIT-CNT microelectrodes after pyrolysis at 900 °C. (d) High-resolution XPS spectrum in the C 1s region of the pyrolyzed carbon microelectrodes after pyrolysis at 900 °C. (e) TGA curve of the PR1-9000A photoresist. (f) Raman spectra of the samples after pyrolysis at 900 and 1,000 °C.

counter microelectrodes were fabricated, and their electrochemical performances were evaluated. Cyclic voltammetry (CV) tests at various scan rates ranging from 10 mV·s$^{-1}$ to 20 V·s$^{-1}$ were carried out to assess the capacitive performance of the micro-supercapacitors using an aqueous $H_2SO_4$ (1 mol·L$^{-1}$) solution as the electrolyte. CV curves of the micro-supercapacitor comprised of C/CHIT-CNT microelectrodes formed at different pyrolysis temperatures and measured at a scan rate of 10 mV·s$^{-1}$ are shown in Fig. 3(a); all the CVs have a rectangular shape, indicating ideal capacitive behavior [1, 18]. As can be seen in Fig. 3(a), the current response of the sample formed by pyrolysis at 900 °C is much higher than those formed at 800 and 1,000 °C at the same scan rate. For the sample pyrolyzed at 900 °C, calculations indicate a high specific capacitance of 6.09 mF·cm$^{-2}$ at a scan rate of 10 mV·s$^{-1}$, much greater than those of the samples prepared at pyrolysis temperatures of 800 °C (0.20 mF·cm$^{-2}$) and 1,000 °C (1.43 mF·cm$^{-2}$). The same tendency was also observed in the CV curves of pure pyrolyzed carbon and C/pristine CNT microelectrode-based superca-pacitors, as shown in Fig. S3 (in the ESM).

The electrochemical performance of micro-supercapacitors was further investigated by galvanos-tatic charge–discharge measurements at different current densities. The charge–discharge curves, shown in Fig. 3(b), at a current density of 0.1 mA·cm$^{-2}$ further confirm that 900 °C is the optimal pyrolysis temperature. The discharge time (59.84 s) of the sample formed by pyrolysis at 900 °C is longer than those of the samples formed at pyrolysis temperatures of 800 and 1,000 °C. Similarly, micro-supercapacitors

containing pure pyrolyzed carbon and C/pristine CNT microelectrodes formed by pyrolysis at 900 °C also had longer discharge times (14.25 and 29.32 s) compared to those pyrolyzed at 800 and 1,000 °C (Fig. S3 in the ESM). It can be concluded that 900 °C is the optimal pyrolysis temperature to fabricate the C/CHIT-CNT composite microelectrodes for micro-supercapacitors.

The CV curves of the micro-supercapacitors formed of different microelectrodes (pure pyrolyzed carbon, C/pristine CNT, and C/CHIT-CNT) at 10 mV·s$^{-1}$ are shown in Fig. 4(a). The largest current response with a C/CHIT-CNT microelectrode-based supercapacitor demonstrates the significant improvement in electro-chemical performance gained by compositing carbon with CHIT-CNT. The specific capacitance of C/CHIT-CNT (6.09 mF·cm$^{-2}$) at a scan rate of 10 mV·s$^{-1}$ is 1.47 times greater than that of pure pyrolyzed carbon (2.47 mF·cm$^{-2}$) and 0.57 times higher than that of C/pristine CNT (3.87 mF·cm$^{-2}$) (Fig. 4(b)). Moreover, the specific capacitance is higher than that of several reported micro-supercapacitors containing carbon-based microelectrodes including photoresist-derived carbon [14, 37], carbide-derived carbon [38], inkjet-printed carbon [39], vertically aligned CNTs [40, 41], graphene films [42], graphene/CNT [43], and reduced graphene oxide/$Fe_2O_3$ [44]. In addition, the charge–discharge curves at a current density of 0.1 mA·cm$^{-2}$ confirm the significant improvement in electrochemical performance (Fig. 4(c)). The discharge time increases from 14.25 to 59.84 s, meaning that more charge is stored by C/CHIT-CNT composite microelectrodes. It is obvious that the performance of the C/CHIT-CNT microelectrode-based micro-supercapacitor is greatly
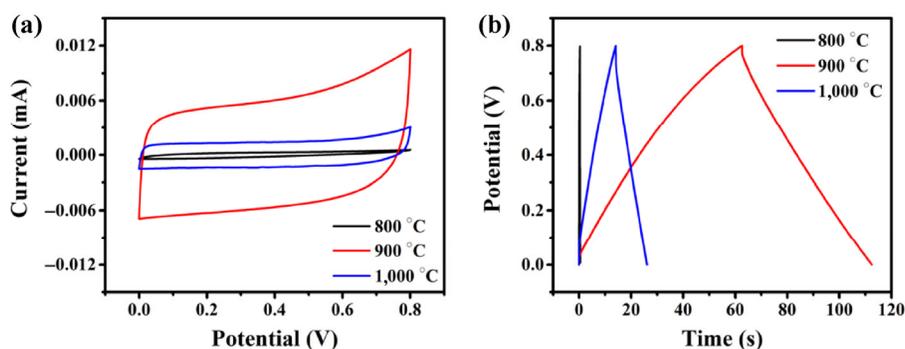


**Figure 3** (a) CV curves of the C/CHIT-CNT microelectrode-based micro-supercapacitor at a scan rate of 10 mV·s$^{-1}$. (b) Galvanostatic charge–discharge profile of C/CHIT-CNT microelectrode-based micro-supercapacitor at a current density of 0.1 mA·cm$^{-2}$.
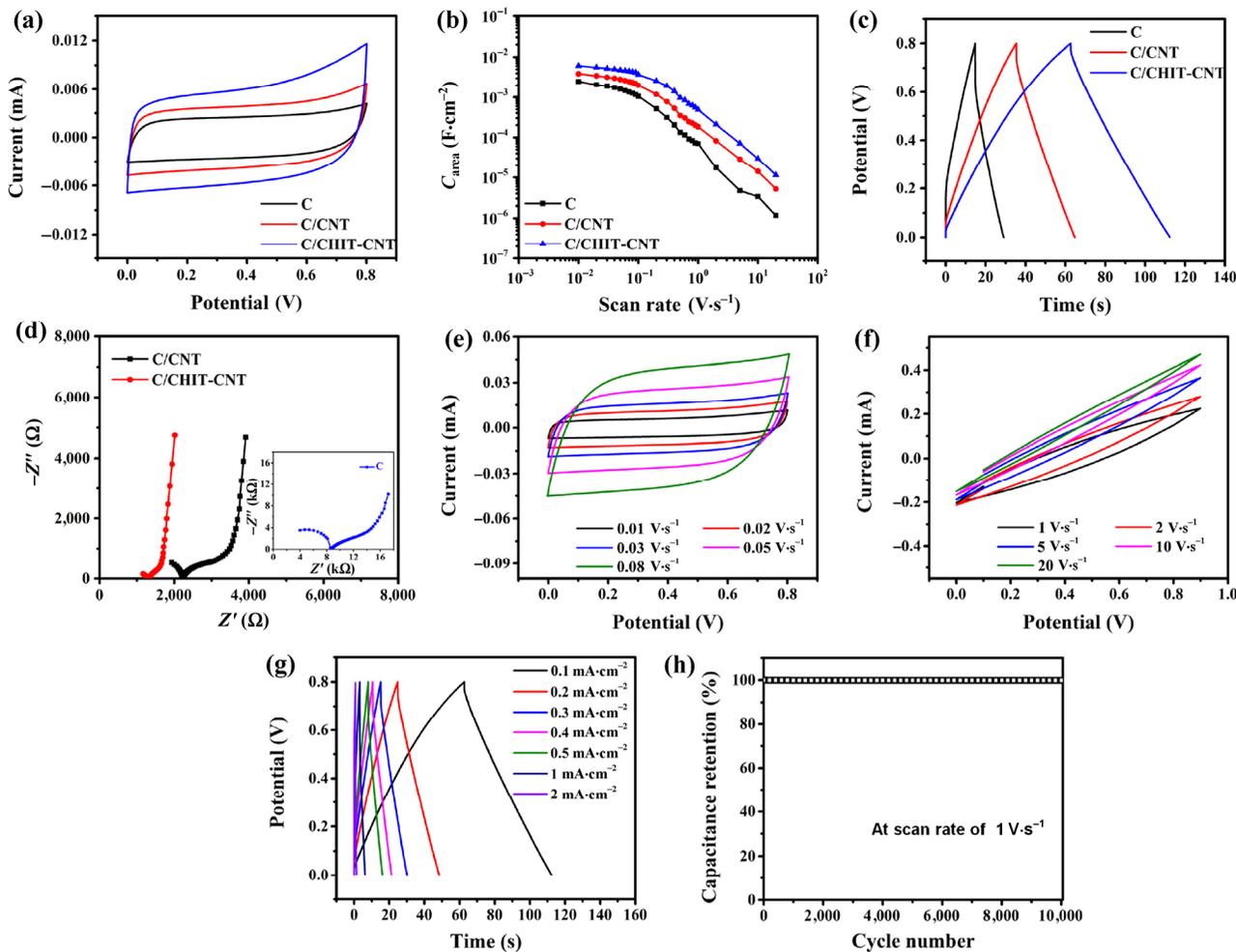
**Figure 4** (a) Comparison of CV curves of micro-supercapacitors with different microelectrodes at a scan rate of 10 mV·s⁻¹. (b) Calculated capacitances of micro-supercapacitors with different microelectrodes at various scan rates. (c) Comparison of the galvanostatic charge–discharge profile of micro-supercapacitors with different microelectrodes at a current density of 0.1 mA·cm⁻². (d) Nyquist plots of micro-supercapacitors with different microelectrodes at frequency from 0.1 Hz to 100 kHz. (e) and (f) CV curves of C/CHIT-CNT microelectrode- based micro-supercapacitor at different scan rates. (g) Comparison of the galvanostatic charge–discharge profile of the C/CHIT-CNT microelectrode-based micro-supercapacitor at different current densities. (h) Cycling stability of C/CHIT-CNT microelectrode-based micro-supercapacitor at a scan rate of 1 V·s⁻¹ over 10,000 cycles.

improved by the compositing process and integration of CNTs, and it is further improved by coating chitosan onto the CNTs. Electrochemical impedance spectroscopy (EIS) measurements were made to evaluate the impedance properties of pure pyrolyzed carbon, C/pristine CNT, and C/CHIT-CNT microelectrodes, respectively. As shown in the corresponding plots (Fig. 4(d)), a high-frequency semicircle is observed, possibly caused by the porous nature of the microelectrodes, i.e., small pores lead to high resistance to ionic transport [37]. The smaller equivalent

series resistance (ESR) values of C/CHIT-CNT microelectrodes also confirm the improvement in electrical transport compared with pure pyrolyzed carbon and C/pristine CNT [7]. The smaller ESR values result from the porous structure of pyrolyzed carbon, which has good conductivity, and their compositing with CNTs, which increases the contact area between electrolyte and electrodes. Furthermore, integration with high specific-surface-area (SSA) CNTs not only improves the electrode conductivity (the electrical conductivity of CNTs is higher than that of pyrolyzed

carbon) but also shortens the path of diffusion for fast-moving electrons [45–48]. The chitosan coating, which is converted to carbon during pyrolysis, prevents agglomeration of CNTs in the matrix. Consequently, a more uniform dispersion of CNTs is obtained, leading to more pathways for electron transport. Furthermore, the obtained carbon layer enhances the contact between the pyrolyzed carbon and CNTs and facilitates ion transport. The C/CHIT-CNT microelectrodes have a high surface area, which accommodates more electrolyte ions, creates more electron pathways, and causes less resistance to electron transport during electrochemical processes. Consequently, outstanding electrochemical performance can be realized by using this microelectrode design and architecture.

The electrochemical performance of the micro-supercapacitor with C/CHIT-CNT microelectrodes was further studied by CV measurements at different scan rates (Figs. 4(e) and 4(f)) and galvanostatic charge–discharge curves at different current densities (Fig. 4(g)). Figure 4(e) shows the CV curves at low scan rates from 10 to 80 mV·s$^{-1}$. The rectangular shape is characteristic of the double-layer capacitance mechanism for charge storage. Furthermore, the current response increased at nearly the same time as the increase in scan rate. This and the calculated specific capacitance, which changes from 6.09 to 4.31 mF·cm$^{-2}$ (Fig. 4(b)), are indications of the good electrochemical stability and high capacitance of the microelectrodes. Because there is insufficient time for ions to diffuse and absorb into the small pores of the pyrolyzed composite at high scan rates, the CV curve deviates from a rectangular shape, accompanied by a decrease in capacitance (Fig. 4(f)). The triangular shapes of charge–discharge curves at different current densities, a typical characteristic of EDLC supercapacitors [9], are consistent with the CV curves. In addition, a very low insulation resistance (iR) drop at each current density from 0.1 to 2 mA·cm$^{-2}$ indicates a low cell resistance, and a capacitance of 7.48 mF·cm$^{-2}$ and a coulombic efficiency of about 95.6% at a current density of 0.1 mA·cm$^{-2}$ were determined. Figure 4(h) shows the cycling performance of C/CHIT-CNT microelectrode-based micro-supercapacitor; little capacitance loss during the cycling process and a remarkable long-term cyclability with 99.9% capacitance retention after 10,000 CV cycles at

a scan rate of 1 V·s$^{-1}$ was observed, demonstrating the excellent cycling performance of the fabricated C/CHIT-CNT microelectrode.

The volumetric energy and power density of micro-supercapacitors with different microelectrodes were calculated from the results of CV measurements, and these are shown in Ragone plots (Fig. 5). At a scan rate of 10 mV·s$^{-1}$, the highest energy density (4.5 mWh·cm$^{-3}$) and highest power density (0.20 W·cm$^{-3}$) were recorded for the C/CHIT-CNT microelectrode-based micro-supercapacitor. The energy density is higher than that of commercial Li-ion thin-film battery [37]. There is a small drop in energy density with increasing power density for the C/CHIT-CNT microelectrode-based micro-supercapacitor. These results demonstrate the advantages of C/CHIT-CNT microelectrodes and are in agreement with CV and galvanostatic charge–discharge data. Furthermore, these results show that this integration strategy is a promising route for the preparation of high-performance C-MEMS-based micro-supercapacitors.
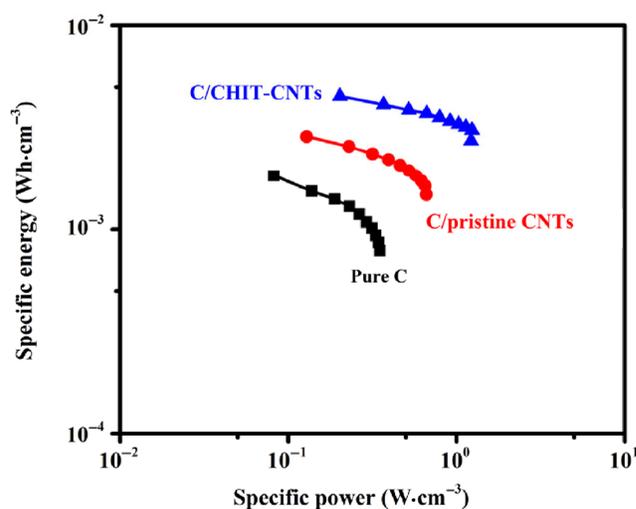


**Figure 5** Ragone plots of the volumetric energy and power density of the fabricated micro-supercapacitors with different microelectrodes.

## 4 Conclusion

In summary, an interdigital micro-supercapacitor with C/CHIT-CNT microelectrodes was fabricated by optimized photolithography and pyrolysis. The excellent electrochemical performance with ultrahigh

specific capacitance and ultra-stable cyclability is attributed to the scalable C-MEMS process and integration of CHIT-CNT. It is significant that our approach enables device fabrication with a composite electrode, simplifying the process. The fine micro-patterning of this composite is suitable for large-scale production and integration with C-MEMS. Furthermore, other kinds of photoresists and inorganic precursors, such as carbon materials and transition metal oxides, can be utilized to explore the potential of this optimized microfabrication process in the development of electrochemical energy storage devices.

## Acknowledgements

**Electronic Supplementary Material**: Supplementary material (XPS survey spectrum of pyrolyzed carbon microelectrodes after 900 ℃ pyrolysis; CV curves of pure C and C/pristine CNTs micro-supercapacitors at a scan rate of 10 mV·s$^{-1}$; galvanostatic charge–discharge profile of pure C and C/pristine CNTs micro-supercapacitors at a current density of 0.1 mA·cm$^{-2}$; synthetic scheme for modification of CNTs by chitosan) is available in the online version of this article at http://dx.doi.org/10.1007/s12274-016-1137-3.

## References

[1] Simon, P.; Gogotsi, Y. Materials for electrochemical capacitors. *Nat. Mater.* **2008**, *7*, 845–854.

[2] Zhang, L. L.; Zhao, X. S. Carbon-based materials as super-capacitor electrodes. *Chem. Soc. Rev.* **2009**, *38*, 2520–2531.

[3] Lin, T. Q.; Chen, I.-W.; Liu, F. X.; Yang, C. Y.; Bi, H.; Xu, F. F.; Huang, F. Q. Nitrogen-doped mesoporous carbon of extraordinary capacitance for electrochemical energy storage. *Science* **2015**, *350*, 1508–1513.

[4] Jiang, H.; Lee, P. S.; Li, C. Z. 3D carbon based nano-structures for advanced supercapacitors. *Energy Environ. Sci.* **2013**, *6*, 41–53.

[5] Wei, L.; Yushin, G. Nanostructured activated carbons from natural precursors for electrical double layer capacitors. *Nano Energy* **2012**, *1*, 552–565.

[6] Wei, L.; Sevilla, M.; Fuertes, A. B.; Mokaya, R.; Yushin, G. Hydrothermal carbonization of abundant renewable natural organic chemicals for high-performance supercapacitor electrodes. *Adv. Energy Mater.* **2011**, *1*, 356–361.

[7] Tian, X. C.; Shi, M. Z.; Xu, X.; Yan, M. Y.; Xu, L.; Minhas-Khan, A.; Han, C. H.; He, L.; Mai, L. Q. Arbitrary shape engineerable spiral micropseudocapacitors with ultrahigh energy and power densities. *Adv. Mater.* **2015**, *27*, 7476–7482.

[8] Liu, W. W.; Lu, C. X.; Wang, X. L.; Tay, R. Y.; Tay, B. K. High-performance microsupercapacitors based on two-dimensional graphene/manganese dioxide/silver nanowire ternary hybrid film. *ACS Nano* **2015**, *9*, 1528–1542.

[9] Beidaghi, M.; Wang, C. L. Micro-supercapacitors based on interdigital electrodes of reduced graphene oxide and carbon nanotube composites with ultrahigh power handling performance. *Adv. Funct. Mater.* **2012**, *22*, 4501–4510.

[10] Wei, L.; Nitta, N.; Yushin, G. Lithographically patterned thin activated carbon films as a new technology platform for on-chip devices. *ACS Nano* **2013**, *7*, 6498–6506.

[11] Jiang, W. C.; Zhai, S. L.; Qian, Q. H.; Yuan, Y.; Karahan, H. E.; Wei, L.; Goh, K.; Ng, A. K.; Wei, J.; Chen, Y. Space-confined assembly of all-carbon hybrid fibers for capacitive energy storage: Realizing a built-to-order concept for micro-supercapacitors. *Energy Environ. Sci.* **2016**, *9*, 611–622.

[12] Beidaghi, M.; Wang, C. L. Micro-supercapacitors based on three dimensional interdigital polypyrrole/C-MEMS electrodes. *Electrochim. Acta* **2011**, *56*, 9508–9514.

[13] Jiang, S. L.; Shi, T. L.; Liu, D.; Long, H.; Xi, S.; Wu, F. S.; Li, X. P.; Xia, Q.; Tang, Z. R. Integration of MnO$_2$ thin film and carbon nanotubes to three-dimensional carbon micro-electrodes for electrochemical microcapacitors. *J. Power Sources* **2014**, *262*, 494–500.

[14] Hsia, B.; Kim, M. S.; Vincent, M.; Carraro, C.; Maboudian, R. Photoresist-derived porous carbon for on-chip micro-supercapacitors. *Carbon* **2013**, *57*, 395–400.

[15] Kaempgen, M.; Chan, C. K.; Ma, J.; Cui, Y.; Gruner, G. Printable thin film supercapacitors using single-walled carbon nanotubes. *Nano Lett.* **2009**, *9*, 1872–1876.

[16] Shen, C. W.; Wang, X. H.; Li, S. W.; Wang, J. G.; Zhang, W. F.; Kang, F. Y. A high-energy-density micro supercapacitor of asymmetric MnO$_2$-carbon configuration by using micro-

fabrication technologies. *J. Power Sources* **2013**, *234*, 302–309.

[17] Chen, W.; Beidaghi, M.; Penmatsa, V.; Bechtold, K.; Kumari, L.; Li, W. Z.; Wang, C. L. Integration of carbon nanotubes to C-MEMS for on-chip supercapacitors. *IEEE T. Nanotechnol.* **2010**, *9*, 734–740.

[18] Wang, H. J.; Peng, C.; Zheng, J. D.; Peng, F.; Yu, H. Design, synthesis and the electrochemical performance of $MnO_2$/C@CNT as supercapacitor material. *Mater. Res. Bull.* **2013**, *48*, 3389–3393.

[19] Kim, S.-K.; Park, H. S. Multiwalled carbon nanotubes coated with a thin carbon layer for use as composite electrodes in supercapacitors. *RSC Adv.* **2014**, *4*, 47827–47832.

[20] Liu, Y. Y.; Tang, J.; Chen, X. Q.; Xin, J. H. Decoration of carbon nanotubes with chitosan. *Carbon* **2005**, *43*, 3178–3180.

[21] Jiang, S. L.; Shi, T. L.; Zhan, X. B.; Xi, S.; Long, H.; Gong, B.; Li, J. J.; Cheng, S. Y.; Huang, Y. Y.; Tang, Z. R. Scalable fabrication of carbon-based MEMS/NEMS and their applications: A review. *J. Micromech. Microeng.* **2015**, *25*, 113001.

[22] Wei, L.; Sevilla, M.; Fuertes, A. B.; Mokaya, R.; Yushin, G. Polypyrrole-derived activated carbons for high-performance electrical double-layer capacitors with ionic liquid electrolyte. *Adv. Funct. Mater.* **2012**, *22*, 827–834.

[23] Sevilla, M.; Mokaya, R. Energy storage applications of activated carbons: Supercapacitors and hydrogen storage. *Energy Environ. Sci.* **2014**, *7*, 1250–1280.

[24] Simon, P.; Gogotsi, Y. Capacitive energy storage in nano-structured carbon-electrolyte systems. *Acc. Chem. Res.* **2013**, *46*, 1094–1103.

[25] Béguin, F.; Presser, V.; Balducci, A.; Frackowiak, E. Carbons and electrolytes for advanced supercapacitors. *Adv. Mater.* **2014**, *26*, 2219–2251.

[26] Futaba, D. N.; Hata, K.; Yamada, T.; Hiraoka, T.; Hayamizu, Y.; Kakudate, Y.; Tanaike, O.; Hatori, H.; Yumura, M.; Iijima, S. Shape-engineerable and highly densely packed single-walled carbon nanotubes and their application as super-capacitor electrodes. *Nat. Mater.* **2006**, *5*, 987–994.

[27] Sivaraman, P.; Bhattacharrya, A. R.; Mishra, S. P.; Thakur, A. P.; Shashidhara, K.; Samui, A. B. Asymmetric super-capacitor containing poly(3-methyl thiophene)-multiwalled carbon nanotubes nanocomposites and activated carbon. *Electrochim. Acta* **2013**, *94*, 182–191.

[28] Penmatsa, V.; Kawarada, H.; Wang, C. L. Fabrication of carbon nanostructures using photo-nanoimprint lithography and pyrolysis. *J. Micromech. Microeng.* **2012**, *22*, 045024.

[29] He, L.; Toda, M.; Kawai, Y.; Miyashita, H.; Omori, M.; Hashida, T.; Berger, R.; Ono, T. Fabrication of CNT-carbon

composite microstructures using Si micromolding and pyrolysis. *Microsyst. Technol.* **2014**, *20*, 201–208.

[30] He, L.; Toda, M.; Kawai, Y.; Sarbi, M. F.; Omori, M.; Hashida, T.; Ono, T. Fabrication of a Si-PZT hybrid XY-microstage with CNT-carbon hinges. *IEEJ Trans. Sens. Micromach.* **2012**, *132*, 425–426.

[31] Zhou, P.; Yang, X.; He, L.; Hao, Z. M.; Luo, W.; Xiong, B.; Xu, X.; Niu, C. J.; Yan, M. Y.; Mai, L. Q. The Young's modulus of high-aspect-ratio carbon/carbon nanotube composite microcantilevers by experimental and modeling validation. *Appl. Phys. Lett.* **2015**, *106*, 111908.

[32] Reserbat-Plantey, A.; Schädler, K. G.; Gaudreau, L.; Navickaite, G.; Güttinger, J.; Chang, D.; Toninelli, C.; Bachtold, A.; Koppens, F. H. L. Electromechanical control of nitrogen-vacancy defect emission using graphene NEMS. *Nat. Commun.* **2016**, *7*, 10218.

[33] Lau, C.; Cooney, M. J.; Atanassov, P. Conductive macroporous composite chitosan-carbon nanotube scaffolds. *Langmuir* **2008**, *24*, 7004–7010.

[34] Yang X. M.; Tu, Y. F.; Li, L.; Shang, S. M.; Tao, X.-M. Well-dispersed chitosan/graphene oxide nanocomposites. *ACS Appl. Mater. Interfaces* **2010**, *2*, 1707–1713.

[35] Lin, J. H.; He, C. Y.; Zhao, Y.; Zhang, S. S. One-step synthesis of silver nanoparticles/carbon nanotubes/chitosan film and its application in glucose biosensor. *Sensor. Actuat.* B **2009**, *137*, 768–773.

[36] Yamamoto, G.; Suk, J. W.; An, J.; Piner, R. D.; Hashida, T.; Takagi, T.; Ruoff, R. S. The influence of Nanoscale defects on the fracture of multi-walled carbon nanotubes under tensile loading. *Diam. Relat. Mater.* **2010**, *19*, 748–751.

[37] Wang, S.; Hsia, B.; Carraro, C.; Maboudian, R. High-performance all solid-state micro-supercapacitor based on patterned photoresist-derived porous carbon electrodes and an ionogel electrolyte. *J. Mater. Chem. A* **2014**, *2*, 7997–8002.

[38] Huang, P. H.; Heon, M.; Pech, D.; Brunet, M.; Taberna, P.-L.; Gogotsi, Y.; Lofland, S.; Hettinger, J. D.; Simon, P. Micro-supercapacitors from carbide derived carbon (CDC) films on silicon chips. *J. Power Sources* **2013**, *225*, 240–244.

[39] Pech, D.; Brunet, M.; Taberna, P.-L.; Simon, P.; Fabre, N.; Mesnilgrente, F.; Conédéra, V.; Durou, H. Elaboration of a microstructured inkjet-printed carbon electrochemical capacitor. *J. Power Sources* **2010**, *195*, 1266–1269.

[40] Hsia, B.; Marschewski, J.; Wang, S.; In, J. B.; Carraro, C.; Poulikakos, D.; Grigoropoulos, C. P.; Maboudian, R. Highly flexible, all solid-state micro-supercapacitors from vertically aligned carbon nanotubes. *Nanotechnology* **2014**, *25*, 055401.

[41] Jiang, Y. Q.; Zhou, Q.; Lin, L. Planar MEMS supercapacitor using carbon nanotube forests. In *Proceedings of the IEEE 22nd International Conference on Micro Electro Mechanical*

*Systems*, Sorrento, Italy, 2009, pp 587–590.

[42] Wu, Z.-S.; Parvez, K.; Feng, X. L.; Müllen, K. Graphene-based in-plane micro-supercapacitors with high power and energy densities. *Nat. Commun.* **2013**, *4*, 2487.

[43] Yun, J.; Kim, D.; Lee, G.; Ha, J. S. All-solid-state flexible micro-supercapacitor arrays with patterned graphene/MWNT electrodes. *Carbon* **2014**, *79*, 156–164.

[44] Gu, S. S.; Lou, Z.; Li, L. D.; Chen, Z. J.; Ma, X. D.; Shen, G. Z. Fabrication of flexible reduced graphene oxide/$Fe_2O_3$ hollow nanospheres based on-chip micro-supercapacitors for integrated photodetecting applications. *Nano Res.* **2016**, *9*, 424–434.

[45] Park, B. Y.; Taherabadi, L.; Wang, C. L.; Zoval, J.; Madou, M. J. Electrical properties and shrinkage of carbonized photoresist films and the implications for carbon micro-electromechanical systems devices in conductive media. *J. Electrochem. Soc.* **2005**, *152*, J136–J143.

[46] Cai, Z. Y.; Xu, L.; Yan, M. Y.; Han, C. H.; He, L.; Hercule, K. M.; Niu, C. J.; Yuan, Z. F.; Xu, W. W.; Qu, L. B. et al. Manganese oxide/carbon yolk–shell nanorod anodes for high capacity lithium batteries. *Nano Lett.* **2015**, *15*, 738–744.

[47] An, Z. L.; He, L.; Toda, M.; Yamamoto, G.; Hashida, T.; Ono, T. Microstructuring of carbon nanotubes-nickel nano-composite. *Nanotechnology* **2015**, *26*, 195601.

[48] Xu, G. H.; Zheng, C.; Zhang, Q.; Huang, J. Q.; Zhao, M. Q.; Nie, J. Q.; Wang, X. H.; Wei, F. Binder-free activated carbon/carbon nanotube paper electrodes for use in supercapacitors. *Nano Res.* **2011**, *4*, 870–881.